Appl. Phys. A 56, 241–248 (1993)

Applied Physics A Solids and Surfaces

Raman Spectra of Single-Crystal C_{60}

M. Matus, H. Kuzmany

Institut für Festkörperphysik und Ludwig Boltzmann Institut für Festkörperphysik, Universität Wien, Strudlhofgasse 4, A-1090 Vienna, Austria
(Fax: +43-1/3103888)

Received 14 November 1992/Accepted 24 December 1992

Abstract. We have analysed the Raman spectra of C_{60} single crystals between room temperature and 10 K and studied the temperature-induced phase transition in this material. The spectra show crystal field splitting of the internal Raman modes but no evidence for a line shift near the phase transition. The photo-induced transformation of the crystals and its implication on the interpretation of the Raman spectra is discussed. In the low temperature phase we observed two lines at 30 cm^{-1} and 41 cm^{-1} which we assign to the librational modes of the crystal.

PACS: 78.30, 61.50.E, 61.80.B

One of the remarkable features of C_{60}, a new allotropic modification of carbon [1], is certainly the possibility to study structural phase transitions under moderate conditions of pressure and temperature. The two other well-known modifications of carbon (diamond and graphite) show such transitions but only at temperatures beyond 1000 K or for pressures in the kilobar region.

Since the early days of fullerene research, Raman spectroscopy proved to be a valuable tool for the investigation of this molecular solid. The existence of only 10 Raman lines [2] together with only 4 IR lines was the first evidence for the exceptional high symmetry of this molecule. Later on Haddon et al. [3] showed Raman spectra to be useful in detecting various phases during alkali metal doping. Recently this technique led to the observation of additional phases in the K–C_{60} system [4, 5].

On the other hand, one has to be careful with the interpretation of Raman experiments on C_{60}. Duclos et al. [6] reported a change of the spectra under the influence of oxygen and laser irradiation. In some more recent work [7] the spectra are claimed to be stable if the fullerene material is highly oxygen free. Other results show the opposite [8]. Whatever the case may be, it is evident that oxygen has a strong influence on various properties of C_{60} [9].

The Raman spectrum of solid C_{60} shows characteristic differences from what one expects for the free molecule. This is not surprising since the crystal field influences the symmetry and force constants. In addition, C_{60}-fullerite shows a structural phase transition [10] from an fcc lattice (space group $Fm3m$) to a sc lattice with four molecules per unit cell (space group $Pa3$) at 260 K. In the high-temperature phase the molecules rotate freely, whereas at low temperatures they freeze at well-defined orientations. This transition can be classified as first order. Early temperature-dependent measurements of Raman spectra on C_{60}/C_{70} thin films [11] showed a kink in the temperature dependence with respect to the line position of the characteristic pinch mode at temperatures around 250 K, but the whole line shift between room temperature and 10 K was just about 1 cm^{-1}. Later experiments on single crystals [7, 12] showed a discontinuous line shift of up to 8 cm^{-1} at temperatures near the phase transition but it remained difficult to understand how the crystal field in the weakly bound van der Waals crystal can influence the strong intramolecular bonds to this extend.

Since the general low quality of the internal crystal structure in thin films of C_{60} is well-known, a detailed analysis of single-crystal material was desirable. Raman lines with smaller widths and sharper phase transitions can be expected [13] and the interaction of the bucky balls with oxygen was expected to be different for bulk material and thin films, respectively. Thus, we studied the temperature- and light-induced changes of the Raman spectra for C_{60} single crystals. Characteristic splittings of the degenerate modes, which, in most cases, extend up to room temperature and a strong temperature dependence of Raman intensities was observed. The increase of intensities is attributed to a change of resonance conditions. The light-induced changes revealed a strong dependence on the exposure of the crystals to ambient conditions and the behavior of the pinch mode was found to be consistent with a two component model.

1 Vibrational Selection Rules

The vibrational modes of C_{60} have been analyzed several years ago [14]. Due to its exceptional high point symmetry (I_h), the free C_{60} molecule shows only 46 distinct vibrational

modes out of $3 \times 60 - 6 = 174$ internal degrees of freedom:

$$\Gamma_{\text{molecule}} = 2A_g(R) + 3T_{1g} + 4T_{2g} + 6G_g + 8H_g(R) + A_u + 4T_{1u}(IR) + 5T_{2u} + 6G_u + 7H_u . \quad (1)$$

Only the 4 T_{1u} modes, and the two A_g modes plus the $8H_g$ modes are visible in the IR-spectrum and in the Raman spectrum, respectively.

In the crystal the high symmetry of the molecule is reduced to the appropriate site symmetry where the molecule is located. However, the frequencies of the internal modes should in general not be so different from the vibrations of the free molecule. The influence of the crystal field may lead to a weak splitting of some of the modes. At room temperature with the free rotating C_{60} spheres one expects the lowest perturbation from the free molecule. The largest subgroup of I_h with an inversion centre is T_h which leads to 37 Raman active modes in 23 I_h derived representations. In the low temperature sc crystal structure the site symmetry of the C_{60} molecules is S_6. From a factor group analysis [15, 16] one finds 145 Raman active modes. Since all considered structures posses a centre of symmetry, Raman activity and IR activity are mutually exclusive. Table 1 summarizes these results.

Since fullerite is a weakly bound van der Waals solid, one expects the frequencies of the external modes in the low energy regime which allows a perturbation treatment [15] for the analysis of the vibrations. For the high temperature phase one finds

$$\Gamma_{\text{ext}} = T_g + T_u , \quad (2)$$

where T_u is the acoustic mode and T_g the libration. In the simple cubic structure the relation is

$$\Gamma_{\text{ext}} = A_g + E_g + 3T_g + A_u + E_u + 3T_u . \quad (3)$$

Here, one T_u is again the acoustic mode and all modes of even symmetry are librations. Thus, the external vibrational modes are Raman silent in both structures, but the librational modes are Raman active. One should therefore observe one libration in the Raman spectra for the high-temperature structure and five librations for the low-temperature structure. However, since the molecules are free rotating at high temperature, the frequency for the libration will be zero.

2 Experimental

C_{60} single crystals with well-defined and very smooth surfaces were grown from the vapor phase using a chromatographically purified starting material. This material was sublimated several times to extract traces of organic solvents. Details of the growing technique and of the crystal quality are described elsewhere in this volume [17].

Raman experiments were performed using a DILOR XY spectrometer equipped with a nitrogen cooled CCD multichannel detector. An argon-ion and a krypton-ion laser were used as excitation sources with wavelengths ranging from 406 nm to 674 nm. Measurements were taken in a back scattering geometry with laser powers in the range of 100 μW. For the bleaching experiments the laser intensity was increased up to 1 mW. Using the idealized relation $d = 4\lambda f/\pi D$ between focal length of the lens f (5 cm), laser beam diameter D (1 mm), laser wavelength λ, and focus diameter d (30 μm), this yields power densities from 14 W/cm^2 to 140 W/cm^2.

Raman spectra were taken from natural crystal faces (mainly {111}) immediately after the crystals were grown and removed from the sealed Pyrex tube. They were mounted on the cold finger of a closed cycle cryostat (Cryotronics) using silver paint. Crystals were not cleaved so as to prevent structural defects and measurements were performed in the temperature range from 10 K to 320 K in a vacuum at approximately 10^{-6} mbar.

For the experiments where the change of the pinch mode with irradiation was studied, the crystals were exposed to ambient conditions for varying periods of time.

Table 1. Even modes of free C_{60}, the high-temperature (HT) and the low-temperature crystal structure (LT), respectively. A_g and H_g for the free molecule and all even modes in the two crystals are Raman active

I_h	T_h (HT)	$4 \times S_6$ (LT)
A_g	A_g	$A_g + F_g$
F_{1g}	F_g	$A_g + E_g + 3F_g$
F_{2g}	F_g	$A_g + E_g + 3F_g$
G_g	$A_g + F_g$	$2A_g + E_g + 4F_g$
H_g	$E_g + F_g$	$A_g + 2E_g + 5F_g$

3 Results

3.1 Photo-Transformation

The photo-transformation of the C_{60} material can be studied by following the behavior of the spectrum in the frequency range of the pinch mode at 1468 cm^{-1}. During the photo-transformation the line at 1468 cm^{-1} decreases and several broader lines appear near to it. From a detailed analysis it can be seen that the new lines do not only appear because the main line is bleached, but grow in absolute intensity. This is demonstrated in Fig. 1 for a thin film sample and for the lines

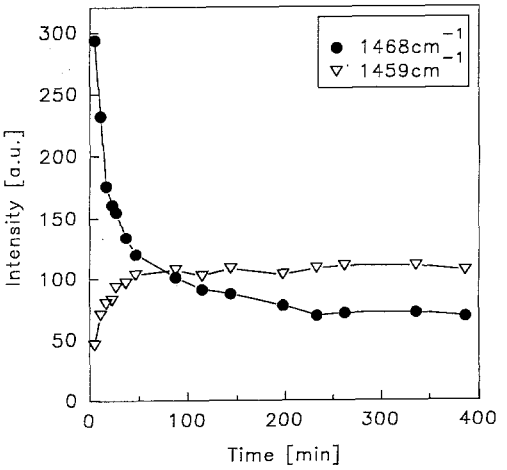

Fig. 1. Intensities of the Raman lines at 1468 cm^{-1} and 1460 cm^{-1} for a thin C_{60} film as a function of laser light exposure in vacuum ($\lambda = 514$ nm)

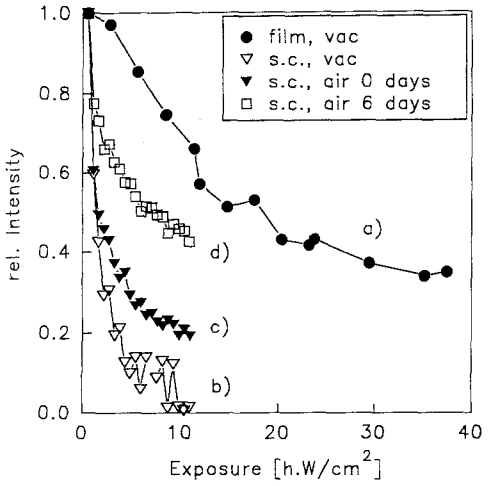

Fig. 2. Relative intensity of the $A_g(2)$ mode as a function of laser light exposure (514 nm). *a* Thin C_{60} film in vacuum, (34 W/cm^2); *b* crystal in vacuum; *c* after removal from glass tube; *d* after exposure of the crystal for 6 days in air (19 W/cm^2)

at 1468 cm^{-1} and 1459 cm^{-1}, respectively. The dynamics of the bleaching process is strongly sample dependent. Figure 2 shows the relative intensity of the 1468 cm^{-1} mode as a function of laser light exposure for four different samples. The top curve (*a*) is for a C_{60} film ($d = 0.4\,\mu$m) on quartz. The sample was stored in air for several weeks. Spectra were taken in vacuum with a laser power density of 34 W/cm^2. The three other curves are for a C_{60} single crystal under different condition. First, the crystal was measured in the sealed evacuated glass tube in which it was prepared (curve *b*). Then the spectrum was taken in air, immediately after removal of the crystal from the quartz tube (curve *c*). The last experiment was performed after keeping the sample for six days in air (curve *d*). In the three measurements on single crystals a laser power density of 19 W/cm^2 was used. It is obvious that storage in air stabilizes the pinch mode against bleaching.

3.2 Intrinsic Raman Lines and Splitting

Figure 3 shows a Raman spectrum from a C_{60} single crystal as obtained at room temperature and at 10 K for two different frequency ranges. The strong lines at 496 cm^{-1} and 1468 cm^{-1} are the A_g-breathing and the A_g-pinch mode, respectively. The other strong lines are the 8 H_g-modes appearing at 273, 430, 710, 774, 1099, 1244, 1428, and 1575 cm^{-1}, respectively. Since in the room temperature spectra the intensities for some H_g-modes are very weak, as e.g., the $H_g(5)$, one can take the positions for the H_g-lines also from the low-temperature spectra. The difference in frequency between the two spectra is only of the order of 1 cm^{-1} if for low temperatures the dominating contribution from the splitted modes is considered only.

As can be seen, lowering the temperature enhances the intensities of the fundamental modes dramatically. In addition to this, many new lines appear, particularly in the frequency range around 1500 cm^{-1}. Also, most of the Raman lines are strongly narrowed which allows observation

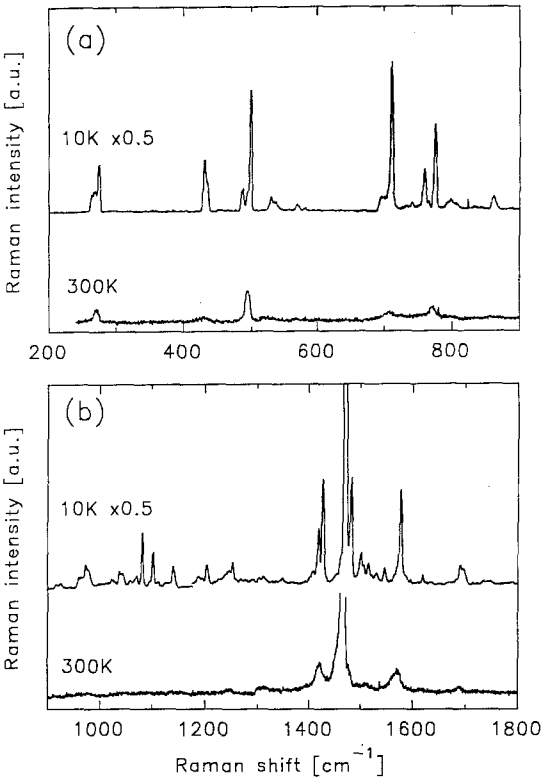

Fig. 3a, b. Raman spectra of a C_{60} single crystal at 300 K and at 10 K, respectively. **a** Low energy region; **b** high energy region (514 nm, 19 W/cm^2)

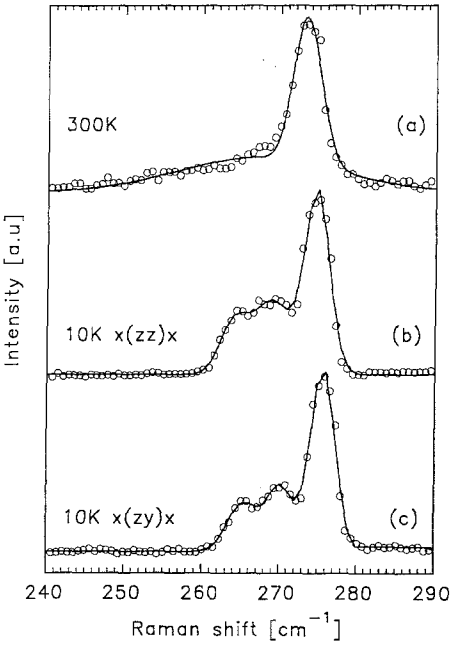

Fig. 4. $H_g(1)$ squashing mode of a C_{60} single crystal. *a* 300 K; *b* 10 K parallel scattering geometry; *c* 10 K perpendicular scattering geometry. The *solid lines* are a fit to the data (514 nm, 19 W/cm^2)

of various splittings of the 5-fold degenerate H_g lines. Up to a maximum of six components of the H_g lines have been observed. As in the case of the A_g modes the splitting of the modes has to be investigated with great care with respect to a bleaching effect or with respect to generation of new

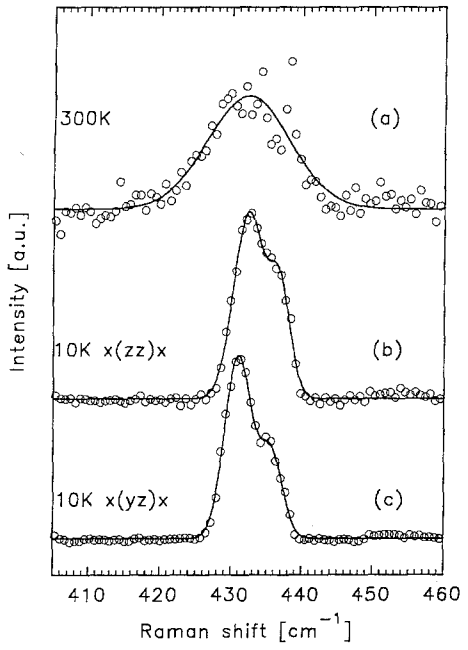

Fig. 5. $H_g(2)$ mode of a C_{60} single crystal. *a* 300 K; *b* 10 K parallel scattering geometry; *c* 10 K perpendicular scattering geometry (514 nm, 19 W/cm^2)

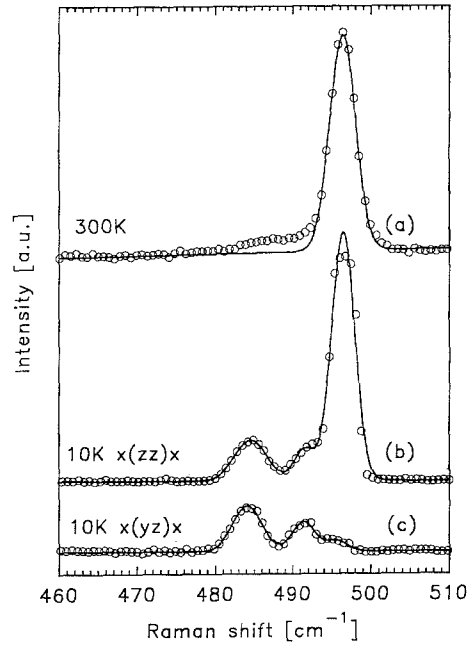

Fig. 6. $A_g(1)$ breathing mode of a C_{60} single crystal. *a* 300 K; *b* 10 K parallel scattering geometry; *c* 10 K perpendicular scattering geometry. *Solid lines* are a fit to the data (514 nm, 19 W/cm^2)

lines due to the illumination. This refers in particular to the experiments near room temperature. The situation at low temperatures is, on the other hand, complicated be the fact that new lines become Raman active and may coincide or nearly coincide with H_g-derived modes.

The lowest energy internal mode ($H_g(1)$, squashing mode) is shown in Fig. 4 in more detail together with a least-square fit of Gaussian line shapes to the data. The top spectrum (*a*) is the squashing mode in the high-temperature structure. The plot is the mean of 70 spectra taken every 10 min. Since the asymmetry did not change during the experiment, we can exclude a photo deterioration as the origin of this broadening. Thus, using a peak fit program we can describe the asymmetric tail as a splitting of the line into two components peaking at 274 cm^{-1} (main peak) and at 266 cm^{-1} (side peak). As can be seen from the figure, the low intensity component is very broad. The two other plots in Fig. 4 are the polarized Raman spectra of the same single crystal at 10 K. The corresponding line positions are 261, 266, and 272 cm^{-1} for both orientations. The widths (FWHM) for all lines are about 4 cm^{-1}.

Figure 5 shows a similar result for the $H_g(2)$ mode. Compared to $H_g(1)$, this line is considerably weaker and has a symmetric line shape at room temperature. At 10 K this line narrows and a splitting into two components occurs.

In Fig. 6 the region around the breathing mode [$A_g(1)$] is shown in more detail. At low temperatures one can observe

Table 2. Observed Raman modes of a C_{60} crystal at 10 K which are assigned to splittings of the fundamental Raman modes of a free molecule. Frequency ω, relative intensity, linewidth (FWHM), and depolarization ratio $\varrho = I_{\parallel\perp}/I_{\parallel\parallel}$ of these modes are shown

ω [cm^{-1}]	Relative intensity	FWHM [cm^{-1}]	ϱ	Assignment referring I_h
492	7	3	0.20	$A_g(1)$
496	56	4	0.010	
1468	1000	4	0.008	$A_g(2)$
261	5	4	0.34	$H_g(1)$
266	8	5	0.30	
272	20	4	0.34	
428	22	5	0.21	$H_g(2)$
433	10	4	0.26	
695	6	8	0.27	$H_g(3)$
706	10	9	0.24	
709	56	4	0.14	
773	35	4	0.26	$H_g(4)$
795	3	13	0.23	
807	2	12	0.14	
1068	4	8	0.30	$H_g(5)$
1080	22	4	0.15	
1097	2	7	0.21	
1101	13	4	0.17	
1109	1	5	0.26	
1215	0.5	2	–	$H_g(6)$
1224	1	11	0.23	
1235	1	4	0.65	
1244	5	18	0.16	
1251	5	3	0.22	
1258	0.3	2	0.60	
1397	0.5	6	–	$H_g(7)$
1408	5	14	0.19	
1417	21	5	0.09	
1425	43	5	0.20	
1432	2	5	0.35	
1545	5	5	0.05	$H_g(8)$
1562	1	4	–	
1573	9	12	0.16	
1576	31	4	0.17	
1585	2	8	0.10	
1594	1	3	–	

a splitting into two components located at 492 cm^{-1} and 496 cm^{-1} with a strong polarization of the latter. The line at 484 cm^{-1} is assigned to an I_h-silent G_g mode which becomes Raman active due to the crystal field. This follows from a comparison of the observed spectra with recent semi-empirical quantum-chemical calculations [18].

Additional support for assignments could be obtained from the determination of depolarization ratios. An example for this is the line at 1480 cm^{-1} just above the pinch mode which increases dramatically with decreasing temperature (Fig. 3), very similar to the H_g modes. Thus it is tempting to assign it to the $H_g(7)$ vibration. However, the depolarization turns out to be very small ($\varrho = 0.03$), typical for an A_g mode. Thus it is not very likely that this line originates from one of the 8 H_g vibrations.

In Table 2 we summarize the data of the A_g- and H_g-derived modes of the low-temperature spectra with respect to their splitting and to the depolarization ratios. The assignment concerning the splitting was again performed by a comparison with the calculations in [18].

3.3 Temperature Dependence of the Raman Lines and External Modes

For some of the Raman lines the temperature dependence was studied with a higher temperature resolution. Figures 7a, b show the two highest energy Raman modes, $H_g(7)$ and $H_g(8)$, at various temperatures. One can see in both cases at least two components with a quite different temperature dependence. For the $H_g(8)$, the high-frequency component of the line is increasing and the low-frequency component is decreasing with decreasing temperature, whereas for the $H_g(7)$ both components increase. This is more clearly demonstrated in Figs. 8a, b and in Fig. 9b, where the intensities from a least-squares fit of two Lorentzian line shapes is presented. Figure 8a shows the intensities for the main line of the $H_g(8)$ mode. The full circles are a plot of the intensities of the high-energy component for an excitation with 40 W/cm^2. Up to a temperature of $\approx$ 260 K the temperature dependence is quite weak. At lower temperatures the slope of the curve increases suddenly up to a maximum around 100 K. Beyond this temperature the intensities level off and eventually decrease. The full lines are a guide for the eye, as described in the discussion. A similar experiment with a power density of 120 W/cm^2 is represented by the open triangles in Fig. 8. The behavior is similar except that the higher phase-transition temperature is shifted downwards by about 15 K, which is probably due to laser heating.

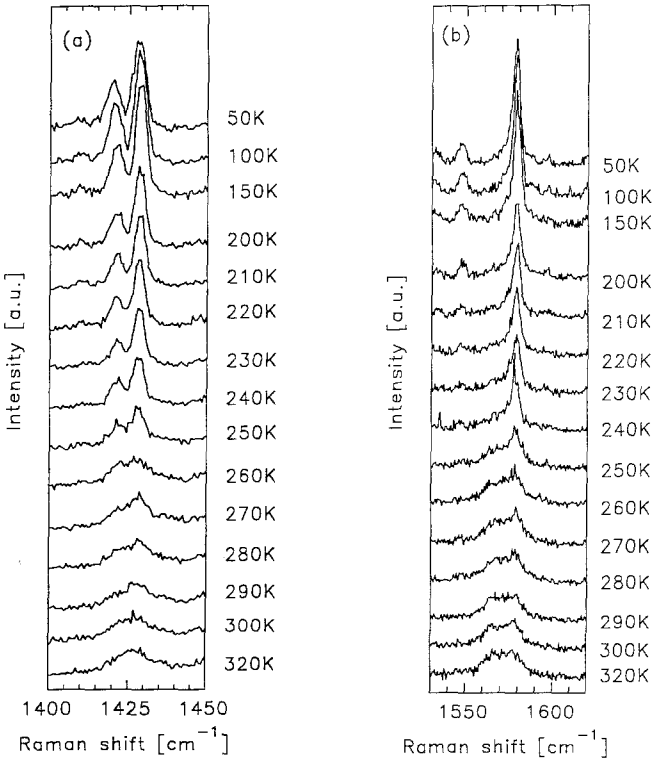

Fig. 7a, b. $H_g(7)$ **(a)** and $H_g(8)$ **(b)** modes of a C_{60} single crystal at different temperatures (514 nm, 40 W/cm^2)

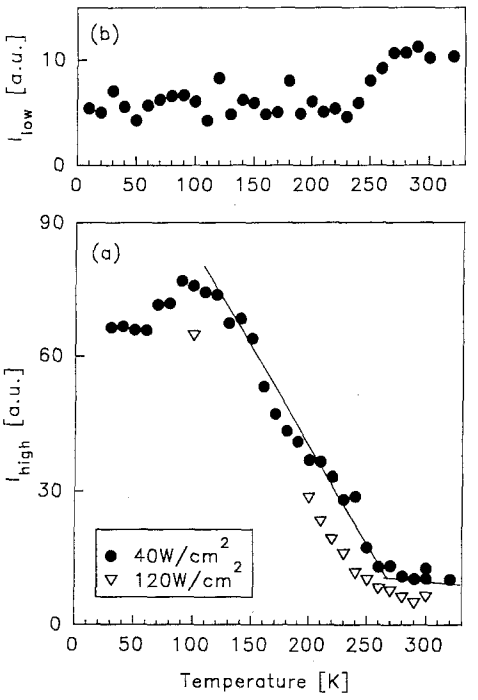

Fig. 8. a Intensity of the higher energy $H_g(8)$ component shown in Fig. 7 as a function of temperature: • 40 W/cm^2, ▽ 120 W/cm^2; **b** intensity of the low-energy component of $H_g(8)$ (514 nm)

The results for the $H_g(7)$ mode in Fig. 9 show basically the same features except that both components of the mode increase with cooling. The characteristic behavior at the higher and lower phase transition is obvious and similar to the one for the $H_g(8)$ mode. Interestingly, the $H_g(7)$ mode exhibits a continuously increasing splitting as shown in Fig. 9b, at least for temperatures below the first-order phase transition.

Figure 10a presents spectra near the $A_g(2)$ mode which were taken at a high laser power density (120 W/cm^2) in order to check any possible line shift or laser radiation effects. At a first glance, the series of spectra look very similar to the behavior of the $H_g(8)$ line. With increasing temperature, the pinch mode becomes weaker and weaker in intensity,

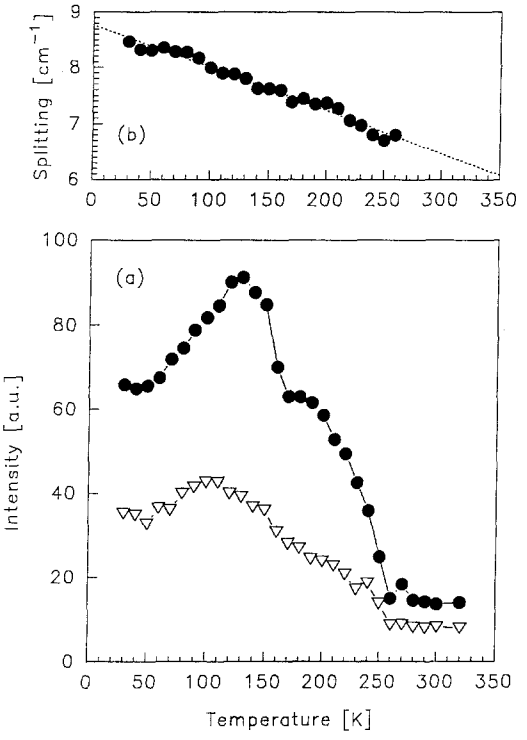

Fig. 9. a Intensities of the two strongest components of the $H_g(7)$ Raman mode as a function of temperature: • higher energy component, ▽ lower energy component; **b** Splitting of the two strongest components of the $H_g(7)$ Raman mode as a function of temperature. The analysis for the frequencies of these modes are unreliable above 260 K because of strong overlapping. The *dashed line* is a linear fit

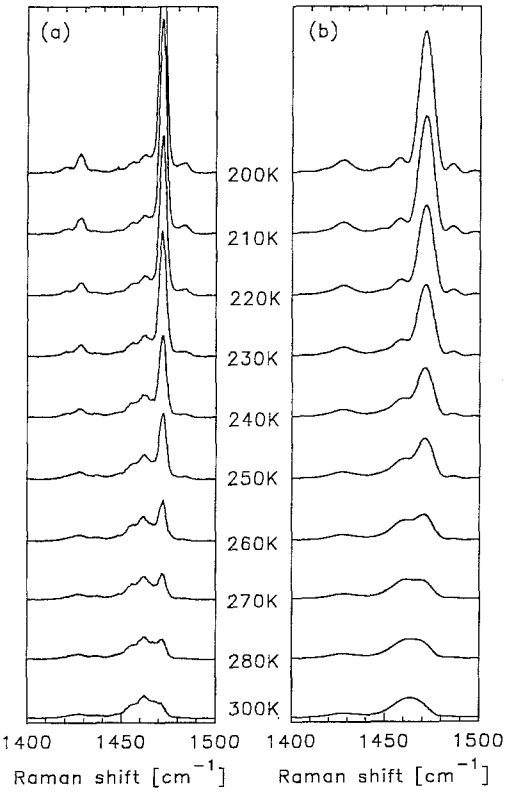

Fig. 10a, b. $A_g(2)$ mode of a C_{60} single crystal at different temperatures (514 nm, 120 W/cm^2). **a** Measured spectra; **b** spectra of **a** smoothened to simulate a lower spectrometer resolution

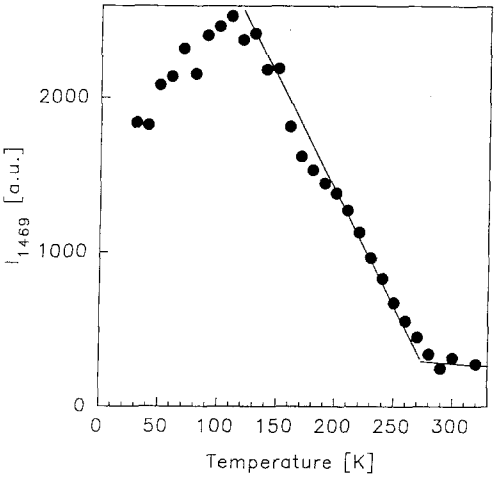

Fig. 11. Intensity of the $A_g(2)$ mode of a C_{60} single crystal as a function of temperature (514 nm, 40 W/cm^2)

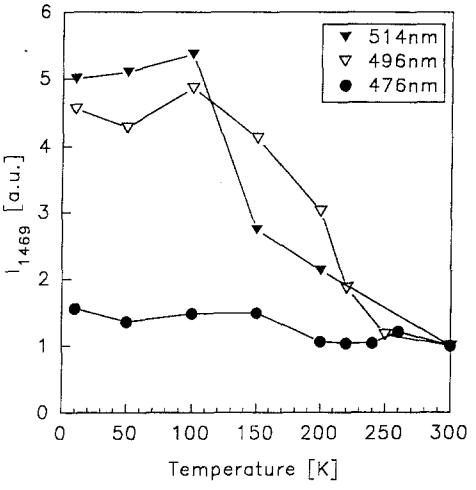

Fig. 12. Relative intensity of the $A_g(2)$ mode of a C_{60} single crystal as a function of temperature for excitation with three different laser wavelengths

whereas the satellite lines on the low-frequency side remain qualitatively unchanged. However, arriving at room temperature, the pinch mode has nearly disappeared which is in strong contrast to measurements taken at room temperature with a very weak laser power. Thus, the photo-degradation process described before is evident. A nonintrinsic line shift can be analyzed if the spectra of Fig. 10a are plotted with a lower resolution as demonstrated in Fig. 10b. In a Raman experiment with weak light excitation the temperature dependence of the line intensity could be followed without bleaching. It is shown in Fig. 11 for a laser power of 40 W/cm^2. The over all behavior is very similar to Fig. 8 and Fig. 9a, even though the kink in the temperature dependence of the intensity at the higher phase transition is shifted upwards by about 20 K.

Since there were arguments that the increase of the line intensities may be due to changes in the resonance conditions, it was important to study the temperature dependence of the spectra for other laser lines as well. Figure 12 shows the relative line intensity of the $A_g(2)$ mode versus temperature for three different laser wavelengths. Raman lines

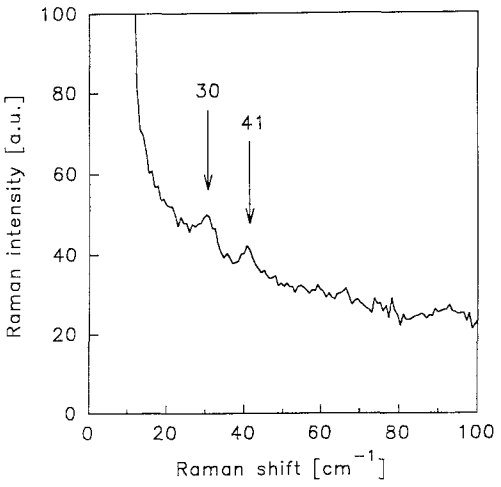

Fig. 13. Low-energy range of the Raman spectrum of a C_{60} single crystal at 10 K. Two lines at 30 cm^{-1} at 41 cm^{-1} can be seen. The broad background is due to the Rayleigh wing (514 nm, 10 W/cm^2)

excited with a laser wavelength in the maximum of the resonance (476 nm) show only a small temperature dependence of the intensities, whereas those on the edge change dramatically.

Finally, the low energy region of the Raman spectrum of a C_{60} single crystal at 10 K is presented in Fig. 13. There are two Raman lines at 30.4 cm^{-1} and 40.9 cm^{-1} close to the Rayleigh wing. The line widths (FWHM) are 4.8 cm^{-1} and 3.5 cm^{-1}, respectively, which compares to the line widths of the higher energy modes. The low-frequency modes could not be observed in all samples.

4 Discussion

The strong influence of the oxygen treatment on the Raman response for the line at 1468 cm^{-1} is clear evidence that it is not intrinsic to the pure C_{60} system. It was argued that it corresponds to the pinch mode of C_{60}, which is slightly disturbed by oxygen as if there was a charge transfer from the oxygen to the fullerene [19]. More recent measurements, where it was possible to obtain a good estimate for the line position of the pinch mode in the neutral C_{60}, confirmed this, but required only a much smaller charge transfer, at least for elevated temperatures [5]. Since, as demonstrated in Fig. 2, the interaction with oxygen stabilizes the response from the pinch mode, the latter may consist of two not very different components. One originates from the intrinsic vibration (pinch mode) and the other from molecules which are stabilized by interaction with oxygen (quasi pinch mode). In the highly oxygen free material, the intrinsic component dominates but decays rapidly with even weak irradiation and a new compound is formed. In the material which was exposed to air for considerable time, the quasi pinch mode dominates and the material appears rather stable. Thus, the more care is taken to prepare the crystals with respect to contamination with oxygen, the more sensitive they become with respect to their stability in Raman excitation. This experimental result has to be considered carefully for the interpretation of frequency shifts as a function of temperature, as, for example, those in Fig. 10a. As demonstrated in Fig. 10b, a frequency shift from 1468 cm^{-1} to 1462 cm^{-1}, appearing rather abruptly at the first-order phase transition, may be observed if the spectral resolution is low. This large shift of 6 cm^{-1} would be difficult to understand from the reasonably well known response of pressure and temperature to the lattice constant on the one hand [20, 21], and from the pressure coefficient for the frequency shift of the pinch mode on the other hand [12]. The reported value for the latter is 4.9 cm^{-1}/GPa, which yields a total frequency shift of about 1 cm^{-1} for the whole frequency range between 0 K and room temperature. This is indeed the range of frequency shifts we observe for the internal modes of the fullerene molecule.

The response of the spectrum for C_{60} crystals is dramatic with respect to changes of the temperature. Two effects have to be discussed: the increase of the number of Raman lines including the splitting of the highly degenerate modes and the general intensity enhancement.

At least 95 Raman modes can be observed in the low temperature phase of C_{60}, which are considered to be a part of the 145 Raman expected modes in the $Fm3m$ structure. It is certainly difficult to assign all lines according to the symmetry species in Table 1. However, some quantitative statements can be given at least for the H_g- and A_g-derived modes compiled in Table 2. At room temperature, the two fully symmetric modes (A_g) show neither a broadening nor a splitting, which is evident from their nondegenerate character. At low temperatures, at least the $A_g(1)$ (referring I_h) line shows a splitting into two components (Fig. 6), which can be assigned to the $A_g + F_g$ representation. The mode with the high depolarization ratio should be the F_g part. The very small depolarization ratio of both A_g lines (Table 2) suggest a small influence of the crystal field on the internal vibrations.

The room-temperature spectra of the H_g modes are broad, asymmetric, or even show a splitting into two components, as seen from the Figs. 4, 5, 7. We assign this behavior to a splitting into the components $F_g + E_g$ according to Table 1. However, the large width for some of the lines suggests some inhomogeneity in the amount of perturbation which leads to the $I_h \rightarrow T_h$ symmetry reduction, or it means that the molecules are not really of T_h symmetry due to an ongoing splitting. The splitting of the lines at room temperature is evidence for crystal-field effects already for the rotating spheres. Lowering the temperature continuously enhances the influence of the crystal field as demonstrated by the increasing splitting in Fig. 9b. This is consistent with a continuous decrease of the lattice constant [22].

The splitting at low temperature is according to Table 1. The maximum observed number of components of the H_g modes is six, which is only two less than predicted by the selection rules. However, since group theory cannot predict accidental degeneracies or line intensities, an observation of a splitting into eight components is an upper limit. All other lines visible in the low-temperature spectra can be assigned to the I_h silent modes (F_{1g}, F_{2g}, and G_g) which become Raman active due to the crystal field [1].

[1] After submission of this paper a detailed description of C_{60} single-crystal Raman spectra was reported by van Loosdrecht et al. [24], where more details of the assignment are given

The changes of the line intensities can be explained by a modification of resonance conditions from a variation of the electronic structure. This variation may originate from decreasing lattice parameters. It is well known [20] that the gap shifts to lower energies under hydrostatic pressure by an amount of 0.08 eV/GPa. Assuming that the influence of temperature on the electronic gap can be modeled by intramolecular distances only, one can estimate the changes in the resonance behavior by the temperature. Taking the values for the compressibility [21] and the thermal expansion [22], a shift of 6 meV in the temperature region from 10 K to 300 K is reasonable. Checking, on the other hand, the shape of the resonance cross section [11], one sees that the green laser sits on the steep edge of the excitation profile. Thus, already small shifts of the gap can enhance the line intensities dramatically. On the other hand, shifting the laser energy to higher values moves the excitation into the peak of the resonance where only a weak temperature dependence of line intensities can be expected. This is indeed observed in Fig. 12.

The linear increase of the line intensities with decreasing temperature, as indicated by the solid line in Fig. 11, is in qualitative agreement with these arguments. The levelling and the final decrease of the intensities below the glass transition can not be explained in this simple manner. Characteristic changes of the electronic structure or of the electron–phonon coupling must be assumed. Since resonance Raman scattering is much more sensitive to such changes as compared to optical spectra, the changes may be observed in the latter only from a very careful analysis.

Lines induced by photo-degradation have a different response to the temperature, as can be seen in Fig. 10a. It means that they do not undergo a resonance excitation with decreasing temperature which confirms their different character in electronic structure. On the other hand, the pinch mode and the quasi pinch mode have the same resonance, which indicates their common origin from the bucky ball.

Lines in the very high energy region of the Raman spectra, like the mode near 1700 cm^{-1} in Fig. 3b, do not show an intensity enhancement comparable to the lines discussed before. It is tempting to assign these lines to overtones.

Although we did not find the two lines at 30 cm^{-1} and 41 cm^{-1} in all samples, there are two arguments to support the suggestion that they are librational modes. Firstly, we never observed the lines in the high-temperature phase. In this phase only one external mode is Raman allowed, but has a zero frequency. Secondly, in recent inelastic neutron scattering experiments on C_{60} single crystals [23], librational modes at 21 cm^{-1}, 29 cm^{-1} and 37 cm^{-1} where observed at a temperature of 200 K. Since we measured at 10 K where a hardening of the modes is expected, the results render the Raman and the neutron data for the librations in very good agreement.

Acknowledgements. This work was supported by the Fonds zur Förderung der Wissenschaftlichen Forschung in Austria, grant P8172. We acknowledge M. Haluška for the preparation of the C_{60} single crystals and we are grateful for valuable discussions with J. Winter and J. Kastner.

References

1. W. Krätschmer, L.D. Lamb, K. Fostiropoulos, D.R. Huffman: Nature **347**, 354 (1990)
2. D.S. Bethune, G. Meijer, W.C. Tang, H.J. Rosen: Chem. Phys. Lett. **174**, 219 (1990)
3. R.C. Haddon, A.F. Hebard, M.J. Rosseinsky, D.W. Murphy, S.J. Duclos, K.B. Lyons, B. Miller, J.M. Rosamilia, R.M. Fleming, A.R. Kortan, S.H. Glarum, A.V. Makhija, A.J. Muller, R.H. Eick, S.M. Zahurak, R. Tycko, G. Dabbagh, F.A. Thiel: Nature **350**, 320 (1991)
4. T. Pichler, M. Matus, J. Kürti, H. Kuzmany: Phys. Rev. B **45**, 13841 (1992)
5. J. Winter, H. Kuzmany: Solid State Commun. **84**, 935 (1992)
6. S.J. Duclos, R.C. Haddon, S.H. Glarum, A.F. Hebard, K.B. Lyons: Solid State Commun. **80**, 481 (1991)
7. P.H.M. van Loosdrecht, P.J.M. van Bentum, G. Meijer: Phys. Rev. Lett. **68**, 1176 (1992)
8. P. Zhou, A.M. Rao, K.-A. Wang, J.D. Robertson, C. Eloi, M.S. Meier, S.L. Ren, X.-X. Bi, P.C. Eklund, M.S. Dresselhaus: Appl. Phys. Lett. **60**, 2871 (1992)
9. M. Matus, H. Kuzmany, E. Sohmen: Phys. Rev. Lett. **68**, 2822 (1992)
10. P.A. Heiney, J.E. Fischer, A.R. McGhie, W.J. Romanow, A.M. Denenstein, J.P. McCauley Jr., A.B. Smith III: Phys. Rev. Lett. **66**, 2911 (1991)
11. M. Matus, H. Kuzmany, W. Krätschmer: Solid State Commun. **80**, 839 (1991)
12. S.H. Tolbert, A.P. Alivisatos, H.E. Lorenzana, M.B. Kruger, R. Jeanloz: Chem. Phys. Lett. **188**, 163 (1992)
13. F. Guggenberger, C. Meingast, R. Heid, P. Adelmann, E. Sohmen, B. Renker, M. Braun, H. Wühl, M. Haluška, H. Kuzmany: Phys. Rev. Lett. (submitted)
14. E. Brendsdal, J. Brunvoll, B.N. Cyvin, S.J. Cyvin: In *Quasicrystals, Network and Molecules of Fivefold Symmetry*, ed. by I. Hargittai (VCH, New York, Weinheim 1990) p 277
15. G. Dresselhaus, M.S. Dresselhaus, P.C. Eklund: Phys. Rev. B **45**, 6923 (1992)
16. P.C. Eklund, P. Zhou, K.-A. Wang, G. Dresselhaus, M.S. Dresselhaus: J. Phys. Chem. Solids **53**, 1391 (1992)
17. M. Haluška, H. Kuzmany, M. Vybornov, P. Rogl, P. Fejdi: Appl. Phys. A **56**, 161–167 (1993)
18. F. Negri, G. Orlandi, F. Zerbetto: Chem. Phys. Lett. **190**, 174 (1992)
19. M. Matus, T. Pichler, M. Haluška, H. Kuzmany: In *Electronic Properties of High-T_c Superconductors*, Springer Ser. Solid-State Sci., Vol. 113 (Springer, Berlin, Heidelberg 1992) (in press)
20. V.K. Dolganov, O.V. Zharikov, I.N. Kremenskaja, K.P. Meletov, Y.A. Ossipyan: Solid State Commun. **83**, 63 (1992)
21. J.E. Fischer, P.A. Heiney, A.R. McGhie, W.J. Romanow, A.M. Denenstein, J.P. McCauley Jr, A.B. Smith III: Science **252**, 1288 (1991)
22. W.I.F. David, R.M. Ibberson, T.J.S. Dennis, J.P. Hare, K. Prassides: Europhys. Lett. **18**, 219 (1992)
23. L. Pintschovius, B. Renker, F. Gompf, R. Heid, S.L. Chaplot, M. Haluška, H. Kuzmany: Phys. Rev. Lett. **69**, 2662 (1992)
24. P.H.M. van Loosdrecht, P.J.M. van Bentum, M.A. Verheijen, G. Meijer: Chem. Phys. Lett. **198**, 587 (1992)